Biopolymer enhancement of drying granular materials
Ruoyu Chen

ice | **proceedings**

Proceedings of the Institution of Civil Engineers
Pages 1–6

Keywords: Biopolymer, Capillary, Desiccation cracks

A two-scale experimental study on the influence of biopolymer enhancement on drying granular materials

Ruoyu Chen, and Manolis Veveakis
Civil and Environmental Engineering, Duke University, Durham, NC, 27708, USA

Cracking resulting from drying (constrained dehydration) poses a significant challenge in geomaterials, impacting their mechanical performance. To address this problem, extensive efforts have been made to prevent or mitigate the occurrence of cracks, with recent attention focused on the utilization of biopolymers. This letter investigates the influence of varying concentrations of the Xanthan biopolymer on the mechanical resopnse of granular materials, examining both macro and micro scales. The strength changes of the soil were evaluated through desiccation experiments, analyzing the appearance and progression of failure on the macro scale. Our findings demonstrate that failure (cracking) progression is mitigated, and eventually eliminated, by increasing the concentration of the additive Xanthan. Additionally, capillary experiments were conducted to assess the changes in attraction and the development of capillary bridges on the micro-scale. They indicate that the formation of hydrogel bridges significantly enhances particle attraction thereby increasing its macro-resistance to cracking.

Introduction

Desiccation cracking is a prevalent phenomenon in drought areas. The formation of cracks increases permeability and generates undesired void volume, thereby altering the mechanical and hydraulic properties. These changes lead to a shortage of agricultural production and deterioration of road infrastructure(Izzo and Miletić (2022); Lee et al. (2019); Liu et al. (2020)).

Numerous research studies have been conducted to analyze the factors that influence desiccation cracks, which can be broadly categorized into external conditions and internal components. The external conditions, including temperature, relative humidity, and basal constraints, play a pivotal role in the development of tensile stress within geomaterials(Chen et al. (2022); Tang et al. (2021); Bin et al. (2009); Peron et al. (2009)). Conversely, the internal components, such as soil admixture materials, possess the potential to adjust the tensile strength(Al-Taie et al. (2016); Kolias et al. (2005); Vail et al. (2020)). Given the challenges associated with controlling external atmospheric conditions in practical applications, there is an increasing interest in exploring economically viable and environmentally sustainable admixture treatments to enhance resistance and mitigate desiccation cracks. One promising option is the utilization of biopolymer, specifically Xanthan, which when mixed into the soil-water mixture has been demonstrated to have no known adverse environmental impacts(Soldo and Miletić (2019)).

The biopolymer-treated soil has been shown in the literature to demonstrate notable improvements in viscosity and strength, as evidenced by a series of tests, including unconfined compression strength, direct shear, and permeability tests (Cabalar et al. (2018); Chen et al. (2015)). Furthermore, the addition of Xanthan to the geomaterial exhibits a reduction in hydraulic conductivity, as reported by Zhang et al. (2022), attributed to bio-clogging whereby Xanthan promotes bonding and induces pore-blocking effects.

Desiccation cracks, arising from tensile failure, can be mitigated if the tensile strength consistently exceeds the effective tensile stress within the geomaterials (Morris et al. (1992); Tang et al. (2021)), a condition that can potentially be achieved through the application of Xanthan. However, to the best of the author's knowledge, the impact of Xanthan on desiccation cracking has not been sufficiently supported by experimental validation. In this letter, we provide such a study, by conducting external atmospheric conditions controlled dehydration tests on a constraint platform with different Xanthan concentrations to reveal the influence of biopolymer and two grains capillary experiments for the insights of force and bonding formations based on fluids with different viscosities.

Material and Method

The (geo)material used in the desiccation tests is granite powder with an average grain size of the order of 50 μm, whose properties are listed in Table.1. Food-grade Xanthan was mixed with distilled water to create fluids with varying viscosities. Four concentrations were prepared: 0% (pure distilled water), 0.1%, 1.0%, and 10.0% (mass concentration). Precise amounts of Xanthan powder and water were measured using a laboratory scale with a division of 0.001g. To prevent potential agglomeration, the fluid was stirred using a hand blender. The specific weight of the prepared fluid was added to the granite powder and thoroughly mixed for the soil samples with constant water content in the desiccation tests.

Table 1. Physical properties of the geomaterial

Specific gravity	Liquid limit	Plastic limit	Young's modulus	Shear modulus	Poisson's ratio
2.892	25.02%	17.15%	8.6Mpa	3.3Mpa	0.2857

All the desiccation and capillary tests were conducted in an atmospheric-controlled chamber with a constant relative humidity(60%) and temperature (25°C). In the desiccation tests, the soil samples are spread on a 90-degree constraint platform with the initial water, instead of the admixture fluid, content set to $34 \pm 2\%$, and the dimension is $150mm \times 50mm \times 14mm$ (length$\times$ width $\times$ height). A precise balance recorded the mass changes during the dehydration process every 10 seconds, and the deformation top surface was captured by a Canon EOS 4000D every minute. The initial water contents were measured by a moisture analyzer, RAD WAG MA 50/1.R. Further details can be found in Ruoyu et al. (2023).

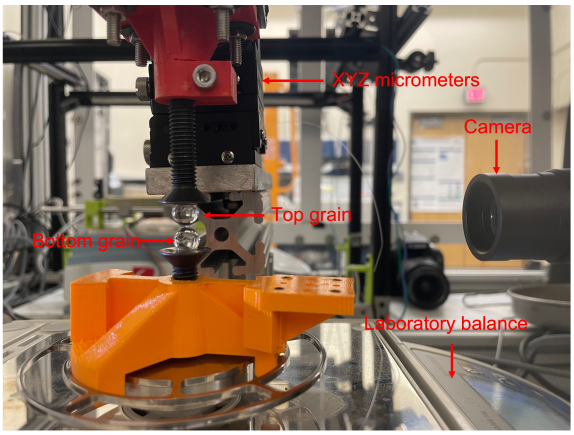

Figure 1. The setup of the capillary system. The entire system was constructed and arranged inside the chamber to ensure consistent environmental conditions.

The capillary experiments involved two glass grains with diameters of 8mm. As depicted in Figure 1, the bottom grain was positioned on a sensitive scale with a readability of $0.0001g$, while the top grain was affixed to a support structure, allowing for the measurement of intergranular force development as the mass changed on the laboratory balance (Mielniczuk et al. (2014); Hueckel et al. (2019)). A volume of $10\mu l$ of the mixed fluid was carefully transferred to the bottom surface of the top grain using a pipettor. The top grain was then gradually lowered until a bridge formed between the two grains, followed by adjusting the separation distance to 0.5mm with the aid of XYZ micrometers. The evolution of capillary bridges and the formation of the bonding (if exists) is captured by a scientific photo camera Basler ACE.

Results and Discussion

The first part of the results focuses on the weight changes and surface images of the drying slabs during the first stage of dehydration, the constant evaporation stage (Tang et al. (2021)). The reason for the stage limitation is that a phase change of Xanthan from fluid to solid is observed during the later stage of dehydration. Additionally, all the cracks show up in this constant evaporation stage, and the water content developments are shown in Fig.2, while the details and values of evaporation rates in these stages can be found in Table.2.

The evaporation rates for the various concentrations exhibit similar values in the targeted stages, contrary to findings from previous studies suggesting that increasing the Xanthan concentration leads to a decrease in evaporation rates (Sorze et al. (2023)). This discrepancy can be explained by the fact that the samples are fully saturated in this constant evaporation stage, and the admixture's impact on the vapor pressure of the fluid, which affects the evaporation flux, is minimal, which follows the formula given by Jafari et al. (2018):

$$\dot{m}_{evap} = \sqrt{\frac{M{\sigma_c}^2}{2\pi R T_v}} \left(\sqrt{\frac{{\sigma_e}^2 T_v}{{\sigma_c}^2 T_l}} P_l - P_v \right) \tag{1}$$

where $\dot{m}_{evap}$ is evaporation rate, M is molar mass of liquid, σ_c and σ_e are empirical evaporation and condensation coefficients, R is the gas constant, T_v and T_l are liquid and vapor temperatures, P_l and P_v are interfacial liquid and vapor pressures. For the Xanthan concentrations in this letter, the changes in M and P_l are neglectable, with other parameters remaining constant during the constant evaporation stages. As shown in Table 2, the evaporation rates during the period from the beginning of the tests to the onset of cracks are approximately the same. The volumetric strain in both the X and Y directions was calculated based on the surface images obtained, revealing a notable disparity in shrinkage volume rates between the samples mixed with pure distilled water and those containing Xanthan fluids.

The second part of the results from the constraint desiccation experiment under the same atmospheric conditions with different

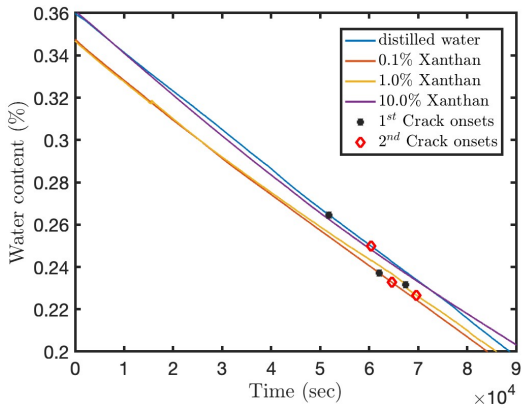

Figure 2. Water content development and crack onsets with different fluids in the same atmospheric conditions

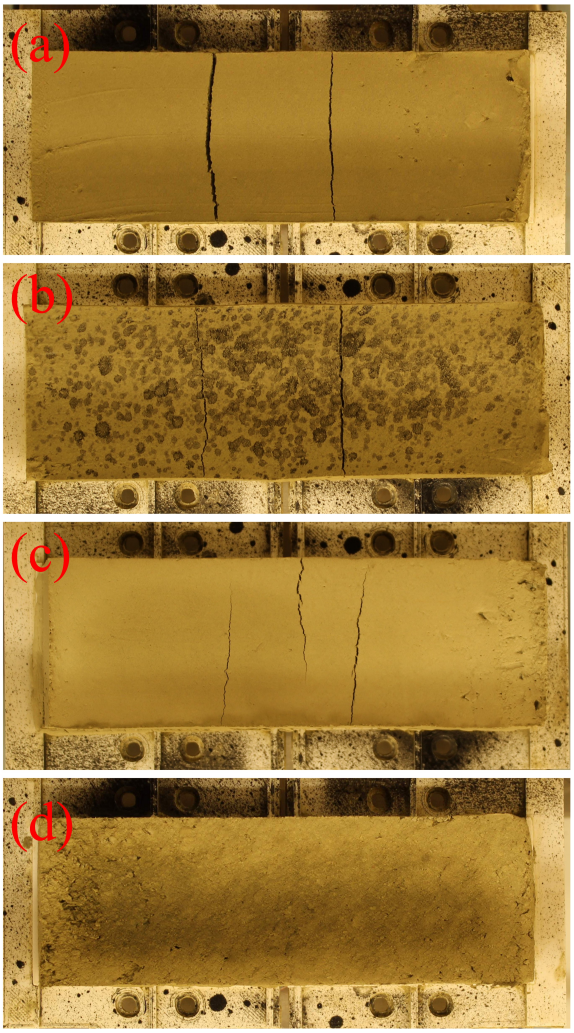

Figure 3. Surface images at the end of tests (no change in the mass of the sample detected for 5 consecutive hours). The fluid is pure distilled water in (a), 0.1% Xanthan in (b), 1.0% Xanthan in (c), and 10.0% Xanthan in (d).

Xanthan concentrations focuses on the numbers and development of cracks. Based on the top surface images, it was observed that the first crack onsets occurred when losing approximately the same amount of water. The numbers of cracks vary between two and three, and the development process shows a bifurcation when the concentration increases to 1.0% and 10.0% shown in Table.2.

Fully developed cracks were identified as cracks that fully penetrated the entire samples, as illustrated in Fig.3(a,b). Nevertheless, the propagation of cracks halted, resulting in a suspension of crack growth, when the biopolymer concentration increased to 1.0%(Fig.3(c)), where the suspension was consistently observed in the reproduced experiments. In the tests with 10.0% Xanthan, the soil samples shrinkage without any appearance of cracks.

The third part of the results from the capillary experiments provides additional support to discuss the shrinkage volume rate and the suspension of cracking. The positive values of the force indicate attractive intergranular forces. The zoom-in figure in Fig.4 reveals that the attraction initially increases and then abruptly drops in the tests of distilled water and 0.1% Xanthan. Instead of reaching zero, a small residual force was found in 0.1% Xanthan, attributed to the remaining Xanthan on the bottom grain(5).

The peak values before the break/rebound are of the same magnitude, $10^{-1}mN$. Also, the capillary bridge broke, which is interpreted as air entry instability (Hueckel et al., 2022; Guevel et al., 2022), around the same time in the tests with distilled water and 0.1% Xanthan. This air entry leads to effective stress concentration and may trigger cracking (Tang et al., 2011).

Meanwhile, instead of dropping to zero for the test with a 1.0% Xanthan concentration, the attraction force rebounds to a value 271 times higher than the initial peak value. Additionally, the force development in 10.0% Xanthan exists a jump right after the injection of fluid to the negative value, which is the repulsion between grains shown as the gap at 120 sec in Fig.4, and then rebound back to the attractive regime. The geometry developments of capillary bridges were presented to explain the intergranular force changes. In the capillary tests conducted with the current setup (volume of fluid and separation distance), most of the capillary bridges were concave except for the initial stage of the 10.0% test. The high viscosity of the fluid in the 10.0% test resulted in an asymmetrical capillary bridge at the initial stage, with a convex meniscus that causes the aforementioned repulsion. The rebound of force in 1.0% and 10.0% Xanthan tests

Table 2. Summary of desiccation results.

Xanthan concentration	Initial void ratio	Evaporation rate (g/s)	Volumetric shrinakge rate (Summation of X and Y direction , mm^3/s)	Number of cracks	Development of cracks
0	1.13	2.56×10^{-4}	1.11×10^{-1}	2	Fully developed
0	1.15	2.19×10^{-4}	9.01×10^{-2}	3	Fully developed
0.1%	1.14	2.52×10^{-4}	1.86×10^{-1}	2	Fully developed
0.1%	1.28	2.11×10^{-4}	1.93×10^{-1}	2	Fully developed
0.1%	1.08	2.33×10^{-4}	1.51×10^{-1}	2	Fully developed
1.0%	1.17	2.39×10^{-4}	1.75×10^{-1}	3	Mitigated
1.0%	1.02	2.57×10^{-4}	1.56×10^{-1}	3	Mitigated
1.0%	1.15	2.61×10^{-4}	1.86×10^{-1}	3	Mitigated
10.0%	1.48	2.25×10^{-4}	1.79×10^{-1}	None	Not found
10.0%	0.73	2.34×10^{-4}	1.51×10^{-1}	None	Not found

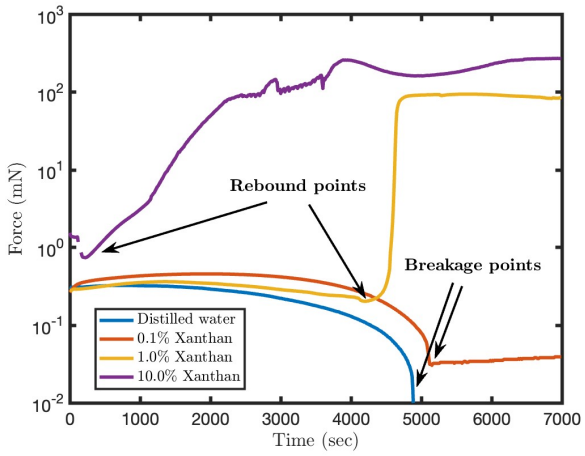

Figure 4. Force development between two grains with different Xanthan concentrations.

is associated with fluid-solid phase changes, while Fig.5 illustrates the development of the capillary bridge at different stages for each group.

The attraction force, or adhesion, is a resultant of Laplace pressure acting along the contact surface and surface tension force along the air-fluid-solid contact lines. The influence of gravity is ignored as it contributed to less than 5% of total intergranular force (Mielniczuk et al., 2014). The simplified surface tension and the Laplace pressure can be obtained following the adjusted formula given by Mielniczuk et al. (2015):

$$F_{Lap} = -\pi r_{neck}^2 \gamma \left(\frac{1}{r_{neck}} + \frac{1}{r_{ext}}\right) \tag{2}$$

$$F_{ST} = 2\pi r_{neck} \gamma \tag{3}$$

in which F_{Lap} is Laplace force, F_{ST} is surface tension force, γ is the surface tension,r_{neck} and r_{ext} are respective the radius of the neck and external radius shown in Fig.5. As water evaporates during the dehydration process, the volume of fluid within the capillary bridges decreases. This reduction in volume causes changes in the geometry of the capillary bridges. And these evolutions of bridge geometry are directly determined by the shifting radii. Additionally, the admixture with Xanthan decreases the surface tension obtained from the Lee–Chan–Pogaku coefficient method and Harkins–Brown correction factors method (Abdulla et al. (2011); Lee et al. (2009)).

The rebound in the 1.0% Xanthan test, presented in Fig.4, results from a unique behavior of the capillary bridge, as it did not narrow till break like in other cases. Instead, the final bridge in the 1.0% Xanthan test survived, primarily consisting of a hydrogel. This hydrogel bridge enhances the overall strength of the structure (Zhang et al., 2022). Furthermore, the same appearance of the hydrogel bridge was observed earlier in higher concentration cases, 10.0% Xanthan, and it provided increased adhesion between the two grains. The force values after rebounds in these two different Xanthan tests indicate that higher concentrations of Xanthan contribute to the formation of a stronger and more adhesive hydrogel bridge. Additionally, vibrations of the resultant were detected in the later stages of the experiments with 1.0% and 10.0% Xanthan. These vibrations could potentially be attributed to the oscillation of the viscous fluid within the capillary bridge. Further investigation is required to comprehensively understand and characterize these vibrations (Bauer and Eidel, 1997).

Conclusion

A series of experiments were conducted to investigate Xanthan's influence on soil's mechanical properties during desiccation, considering two different scales. The experimental results encompass various aspects, including evaporation rates, shrinkage rates, crack appearance and development from desiccation tests, as well as the intergranular force changes and morphology in capillary tests.

The addition of Xanthan alters the volumetric shrinkage rates, while no significant differences are found in evaporation rates within the

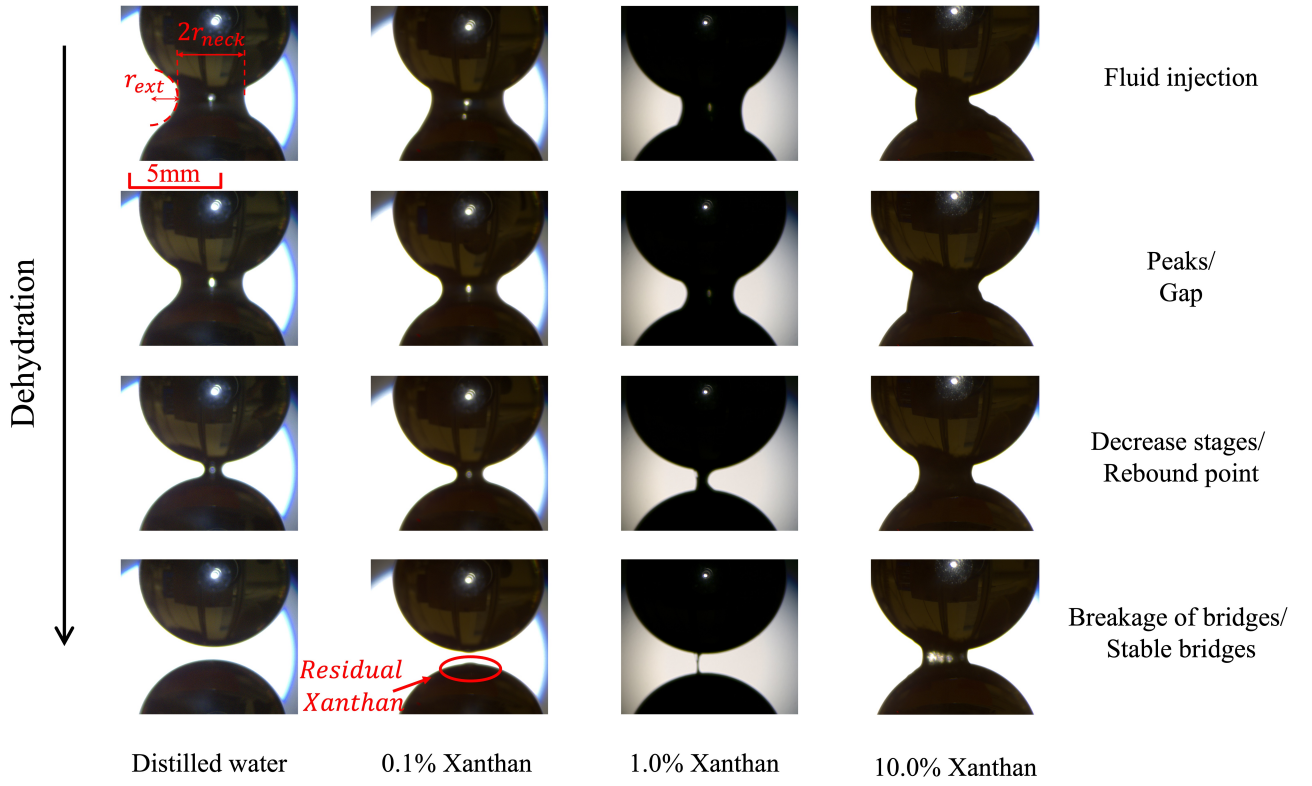

Figure 5. Force development between two grains with different Xanthan concentrations.

concentration range of 0% to 10% during the constant evaporation stages. The development of cracks was suspended in soil samples amended with higher concentrations of Xanthan.

A bonding was found in the capillary tests with 1.0% and 10.0% Xanthan, which correspond to the presence of residual forces during the dehydration process. And the increment of intergranular force followed by a sudden jump and the water bridge breakage was observed in the capillary tests with distilled water and low Xanthan concentration (0.1%).

These experimental results provide valuable insights into understanding the mechanical behavior of Xanthan-amended geomaterials and open up further investigation at the mesoscale to establish a comprehensive understanding and bridge the gap between micro-scale capillary results and macro-scale desiccation responses.

Acknowledgements

The authors gratefully acknowledge the support of the U.S. Department of Energy grant DE-NE0008746 and the U.S. National Science Foundation for project CMMI-2042325.

REFERENCES

M. Z. Izzo, M. Miletić, Desiccation cracking behavior of sustainable and environmentally friendly reinforced cohesive soils, Polymers 14 (2022) 1318.

S. Lee, M. Chung, H. M. Park, K.-I. Song, I. Chang, Xanthan gum biopolymer as soil-stabilization binder for road construction using local soil in sri lanka, Journal of Materials in Civil Engineering 31 (2019) 06019012.

B. Liu, C. Zhu, C.-S. Tang, Y.-H. Xie, L.-Y. Yin, Q. Cheng, B. Shi, Bio-remediation of desiccation cracking in clayey soils through microbially induced calcite precipitation (micp), Engineering geology 264 (2020) 105389.

R. Chen, W. Lindqwister, T. Hueckel, M. Veveakis, An experimental study on silt desiccation cracking with different basal constraints and various humidity, in: Multiscale Processes of Instability, Deformation and Fracturing in Geomaterials: Proceedings of 12th International Workshop on Bifurcation and Degradation in Geomechanics, Springer, 2022, pp. 144–154.

C.-S. Tang, C. Zhu, Q. Cheng, H. Zeng, J.-J. Xu, B.-G. Tian, B. Shi, Desiccation cracking of soils: A review of investigation approaches, underlying mechanisms, and influencing factors, Earth-Science Reviews 216 (2021) 103586.

S. Bin, T. Chao-sheng, W. Bao-jun, J. Hong-tao, Development and mechanism of desiccation cracking of clayey soil under different temperatures, Geological Journal of China Universities 15 (2009) 192.

H. Peron, L. Laloui, T. Hueckel, L. B. Hu, Desiccation cracking of soils, European journal of environmental and civil engineering 13 (2009) 869–888.

A. Al-Taie, M. M. Disfani, R. Evans, A. Arulrajah, S. Horpibulsuk, Swell-shrink cycles of lime stabilized expansive subgrade, Procedia engineering 143 (2016) 615–622.

S. Kolias, V. Kasselouri-Rigopoulou, A. Karahalios, Stabilisation of clayey soils with high calcium fly ash and cement, Cement and Concrete Composites 27 (2005) 301–313.

M. Vail, C. Zhu, C.-S. Tang, N. Maute, M. T. Montalbo-Lomboy, Desiccation cracking behavior of clayey soils treated with biocement and bottom ash admixture during wetting–drying cycles, Transportation Research Record 2674 (2020) 441–454.

A. Soldo, M. Miletić, Study on shear strength of xanthan gum-amended soil, Sustainability 11 (2019) 6142.

A. Cabalar, H. Mohammed, M. Khalaf, Geotechnical properties of a low-plasticity clay with biopolymer, Journal of Materials in Civil Engineering 30 (2018). doi:10.1061/(ASCE)MT.1943-5533.0002380.

R. Chen, I. Lee, L. Zhang, Biopolymer stabilization of mine tailings for dust control, Journal of geotechnical and geoenvironmental engineering 141 (2015) 04014100.

J. Zhang, Z. Meng, T. Jiang, S. Wang, J. Zhao, X. Zhao, Experimental study on the shear strength of silt treated by xanthan gum during the wetting process, Applied Sciences 12 (2022) 6053.

P. H. Morris, J. Graham, D. J. Williams, Cracking in drying soils, Canadian Geotechnical Journal 29 (1992) 263–277.

C. Ruoyu, L. Winston, H. Tomasz, M. Veveakis, The physics of desiccation cracks 1: ductile fracturing and dependence on relative humidity, 2023. Submitted to Geomechanics for Energy and the Environment.

B. Mielniczuk, T. Hueckel, M. S. E. Youssoufi, Evaporation-induced evolution of the capillary force between two grains, Granular Matter 16 (2014) 815–828.

T. Hueckel, B. Mielniczuk, M. Youssoufi, Adhesion-force micro-scale study of desiccating granular material, Géotechnique 70 (2019) 1–45. doi:10.1680/jgeot.18.p.298.

A. Sorze, F. Valentini, A. Dorigato, A. Pegoretti, Development of a xanthan gum based superabsorbent and water retaining composites for agricultural and forestry applications, Molecules 28 (2023) 1952.

P. Jafari, A. Masoudi, P. Irajizad, M. Nazari, V. Kashyap, B. Eslami, H. Ghasemi, Evaporation mass flux: a predictive model and experiments, Langmuir 34 (2018) 11676–11684.

T. Hueckel, B. Mielniczuk, A. Guével, M. Veveakis, Capillary water in 2-d drying—cracking sub-grain scale soil models: Dynamics and instabilities of haines jumps, Water Resources Research 58 (2022) e2022WR033246. URL: https://agupubs.onlinelibrary.wiley.com/doi/abs/10.1029/2022WR033246. doi:https://doi.org/10.1029/2022WR033246. arXiv:https://agupubs.onlinelibrary.wiley.com/doi/pd e2022WR033246 2022WR033246.

A. Guevel, B. Mielniczuk, M. Veveakis, T. Hueckel, Life expectancy of evaporating capillary bridges predicted by tertiary creep modeling, Frontiers in Mechanical Engineering 8 (2022). URL: https://www.frontiersin.org/articles/10.3389/fmech.2022.838501. doi:10.3389/fmech.2022.838501.

C.-S. Tang, B. Shi, C. Liu, W.-B. Suo, L. Gao, Experimental characterization of shrinkage and desiccation cracking in thin clay layer, Applied Clay Science 52 (2011) 69–77.

B. Mielniczuk, T. Hueckel, M. S. El Youssoufi, Laplace pressure evolution and four instabilities in evaporating two-grain liquid bridges, Powder Technology 283 (2015) 137–151.

R. Abdulla, E. S. Chan, P. Ravindra, Biodiesel production from jatropha curcas: a critical review, Critical Reviews in Biotechnology 31 (2011) 53–64.

B.-B. Lee, P. Ravindra, E.-S. Chan, New drop weight analysis for surface tension determination of liquids, Colloids and Surfaces A: Physicochemical and Engineering Aspects 332 (2009) 112–120.

H. F. Bauer, W. Eidel, Axisymmetric viscous liquid oscillations in a cylindrical container, Forschung im Ingenieurwesen 63 (1997) 189–201.